ARTICLES

Control of vortex breakdown by addition of near-axis swirl

Hyder S. Husain, Vladimir Shtern, and Fazle Hussain
University of Houston, Houston, Texas 77204-4006

(Received 24 June 2002; accepted 27 August 2002; published 19 December 2002)

We present a new method for controlling *vortex breakdown* (VB) via addition of co- or counter-rotation near the axis. Co-rotation is adequate to totally suppress VB, whereas counter-rotation increases the number and size of VB ''bubbles'' and makes the flow unsteady. We study these effects in a closed cylindrical container, in which a rotating end disc drives the base flow; an independently rotating central rod (with rod radius$\ll$disk radius) is employed to control VB. This flow, being free of ambient disturbances, is well suited for understanding both the VB mechanism and its control; the present work appears to be the first to study VB *control*. We develop and explain our control strategy using flow visualization and simple analytical reasoning. Our results suggest that an additional co- or counter-rotation, applied near the vortex axis, can be effective in suppressing or enhancing VB in practical flows. © *2003 American Institute of Physics.*
[DOI: 10.1063/1.1530161]

I. INTRODUCTION

Vortex breakdown (VB)—an abrupt expansion of a slender vortex into an axisymmetric ''bubble'' or a helical flow pattern[1]—occurs in many practical flows. VB control (suppression or stimulation) is therefore of fundamental interest and has important applications, discussed below.

A. Vortex breakdown in practical flows

VB is crucial in delta-wing aircraft, vortex burners, vortex reactors, and vortex suction devices. VB on a delta wing causes (i) an abrupt drop in lift, (ii) an increase in drag, and (iii) the development of a rolling moment; these effects can cause the loss of aircraft control.[2] In contrast, VB is beneficial in vortex reactors and burners,[3] providing efficient mixing and stable combustion because a VB bubble acts as a flame holder. In vortex suction devices, VB helps collect hazardous emissions.[4]

In addition to these applications, an induced VB can destroy wing-tip vortices of a large aircraft, which are hazardous to trailing aircraft. A control strategy, involving even a strong additional swirl near the vortex axis is feasible and affordable, as this control is required only during take-off and landing.

While VB control in burners and reactors can be realized by an appropriate selection of flow parameters (e.g., swirl-to-axial velocity ratio) and geometry (e.g., variation of the wall radius along the axis), control becomes problematic in rapidly changing flows, e.g., during aircraft maneuvers (when for safety, VB must be either suppressed completely or shifted downstream of the wings). Control of the location of VB via blowing[5] has been based on engineering intuition only and appears unrealistic for wing-tip vortices. A fundamental basis for VB control is yet to be developed.

The prediction and control of VB is difficult because of many parameters involved, e.g., swirl-to-axial velocity ratio, external axial pressure gradient, flow divergence angle, and upstream flow profile.[5] Changes in these parameters, as well as external disturbances, strongly influence VB. Basic research aimed at developing a VB control strategy requires a well-defined and well-controlled flow. This motivates us to choose a confined flow, free of external disturbances.

B. Vortex breakdown in a closed cylinder

There are several advantages to studying VB in a confined flow. First, the role of control parameters can be clarified in the absence of unpredictable ambient disturbances. Second, boundary conditions are well defined, allowing meaningful comparisons of experimental[6] and numerical[7] results. Understanding of the flow physics and the means of VB control can then be extended to practical flows, confined or open.

Escudier's studies[6] in a closed cylindrical container revealed a variety of VB patterns and their dependence on the aspect ratio H/R_d and the disk Reynolds number $\mathrm{Re}_d = \Omega_d R_d^2/\nu$ (ν is the kinematic viscosity, H is the cylinder height, R_d is the cylinder radius, and Ω_d is the angular speed of the disk). To explore the VB mechanism, other researchers have modified this base flow in different ways. Spohn *et al.*[8] and Young *et al.*[9] studied a flow in a cylinder driven by its rotating bottom disk, with the top surface being free. Experimental[10] and numerical[11,12] studies have employed independent rotation of both end disks. Goldshtik *et al.*[13] and Bradlaw[14] investigated the effects of independent rotation of the bottom disk and the cylinder wall. Pereira *et al.*[15] replaced the rotating disk by a cone. Mullin *et al.*[16] used a

 © 2003 American Institute of Physics

Downloaded 14 Apr 2006 to 129.7.158.43. Redistribution subject to AIP license or copyright, see http://pof.aip.org/pof/copyright.jsp

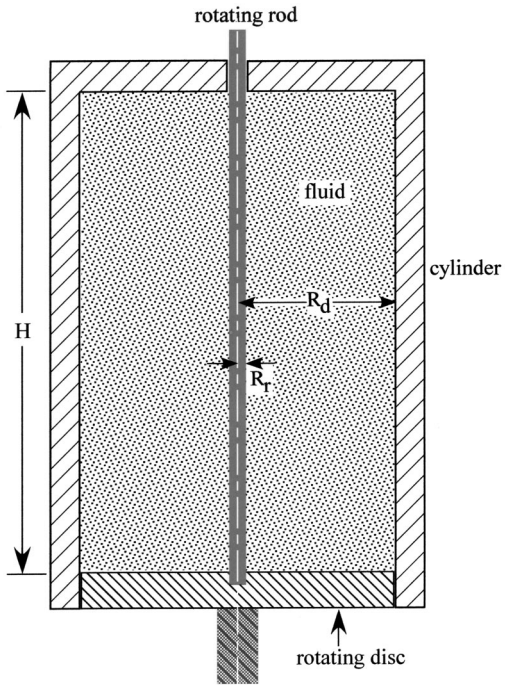

FIG. 1. Schematic of the flow facility.

cylindrical or conical central body which was stationary or rotating together with the rotating disk. We will discuss this closest-to-our study at the end of our paper and explain why our results contradict the conclusions by Mullin *et al.*[16] These works have not addressed VB control, the objective of our study.

We study a new means of VB control—by the addition of near-axis counter-rotation or co-rotation with the help of a thin central rod. In the remainder of the paper we describe the experimental apparatus and procedure (Sec. II), examine the effects of the rod co-rotation (Sec. III) and counter-rotation (Sec. IV), compare our findings with those of Mullin *et al.*[16] (Sec. V) and summarize the results (Sec. VI).

II. EXPERIMENTAL APPARATUS AND PROCEDURE

The experimental apparatus, shown in Fig. 1, consists of a 91.5 cm long glass cylinder of inner radius $R_d=7.62$ cm and a central rod of radius $R_r=0.317$ cm (subscripts d and r refer to the rotating disk and the rod, respectively). The top disk and the sidewall of the cylinder are stationary while the bottom disk rotates. The rod and the bottom disk rotate independently, either in the same (co-rotation) or opposite (counter-rotation) directions. Stepping motors control the disk and rod rotation speeds.

For convenient comparison with prior experimental[6] and numerical[7] results, we chose $\mathrm{Re}_d=2720$ and $H/R_d=3.25$. At these parameter values, the base flow has a steady VB with three vortex rings (denoted as *i*, *ii*, and *iii* in Fig. 2). A homogeneous mixture of glycerin (77% by volume) and water (23%) was used at temperature 23.5 °C with $\nu=50$ cSt. To control VB, we varied the rod Reynolds number Re_r $(\equiv|\Omega_r|R_r^2/\nu)$ from 0 to 29 for co-rotation and from 0 to 16.5 for counter-rotation; Ω_r is the rod angular velocity.

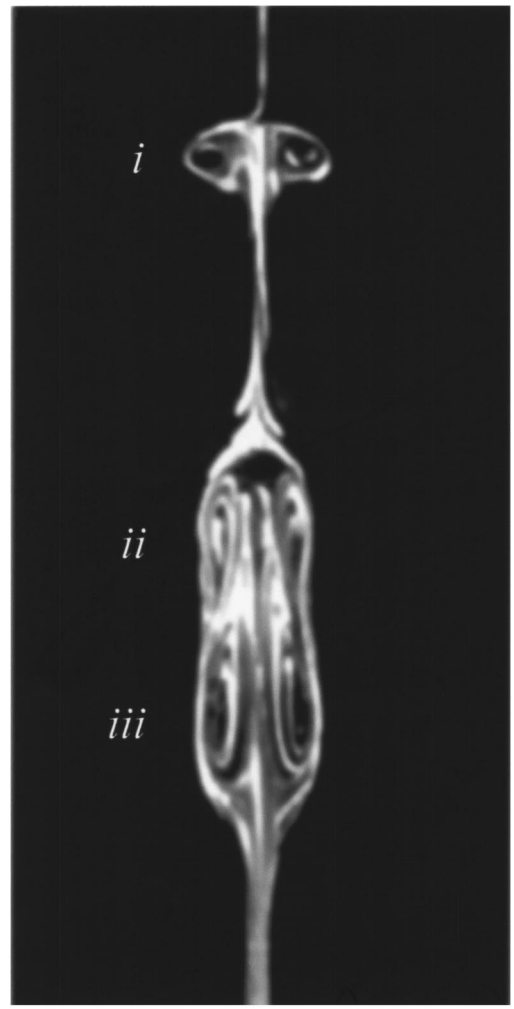

FIG. 2. Flow visualization showing three vortex rings (*i*–*iii*) without the central rod at $\mathrm{Re}_d=2720$ and $H/R_d=3.25$.

We visualized the flow by a laser-induced-fluorescence technique employing a 12-W Ar-ion laser. The laser beam, flared into a sheet of about 0.5 mm thickness, was parallel to a meridional plane of the cylinder. The light sheet was slightly shifted from the axis to avoid reflection by the rod and hence obtain clear visualization pictures. A fluorescent dye (Fluorescein) dissolved in the glycerin–water solution was seeped in through a small hole (1 mm diameter) in the top disk close to the rod. In addition, to verify the observed flow pattern, polystyrene particles (5 μm size; specific gravity 1.04, i.e., the particles are nearly neutrally buoyant) mixed with a sample glycerin–water solution, were injected through a thin tube in the regions of expected near-axis locations of vortex rings. A comparison with prior experiments[6] and numerical simulations[7] showed good consistency of the flow pattern inferred from flow visualization.

The stationary rod, being thin $(R_r/R_d\approx 0.04)$, insignificantly changes the base flow, as comparison of Fig. 2 (without the rod) and Fig. 3(a1) (with the rod) shows. In both cases, the flow has a steady VB with three vortex rings of nearly the same sizes and locations. In contrast, the

Downloaded 14 Apr 2006 to 129.7.158.43. Redistribution subject to AIP license or copyright, see http://pof.aip.org/pof/copyright.jsp

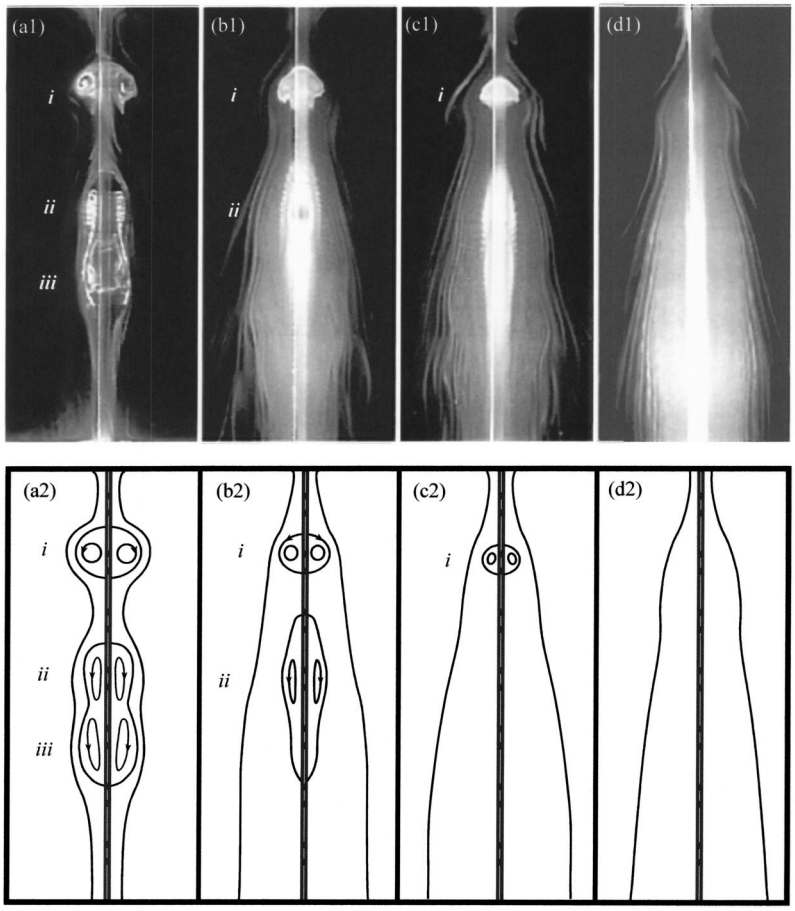

FIG. 3. Flow visualization (1) and the corresponding schematics (2) show the effect of co-rotating rod on vortex breakdown with increasing Re_r. (a) $\mathrm{Re}_r=0$; (b) $\mathrm{Re}_r=12$; (c) $\mathrm{Re}_r=21$; and (d) $\mathrm{Re}_r=29$. Arrows in the schematics indicate the flow direction.

rod rotation significantly affects the flow, as discussed below.

III. CO-ROTATION

A. Experimental observations

Figure 3 shows how the VB disappears as Re_r of the rod co-rotation increases: the flow patterns are clearly distinct at $\mathrm{Re}_r=0$ (a1), 12 (b1), 21 (c1), and 29 (d1). The schematics in the bottom row—Figs. 3(a2)–3(d2)—illustrate our interpretation of the flow pattern (based on the flow observation at different values of Re_r as well). The curves show stream surfaces outside, at the boundary, and inside the VB region.

As Re_r increases starting from 0, the lowest vortex ring (*iii*) approaches the rod and then vanishes completely at $\mathrm{Re}_r=12$, while vortex rings *i* and *ii* shrink [compare Figs. 3(a) and 3(b) and note that the change in *ii* is more significant than that in *i*]. As Re_r increases from 12 to 21, the next vortex ring (*ii*) vanishes while vortex *i* continues to shrink [compare Figs. 3(b) and 3(c)]. Finally, as Re_r reaches 29, vortex *i* disappears completely [compare Figs. 3(c) and 3(d)]. With further increase in Re_r, no change in the flow topology occurs while stream surfaces become less wavy (we examined this up to $\mathrm{Re}_r=40$). Also, by introducing polystyrene particles, we found no VB bubble for $\mathrm{Re}_r>29$. Thus, VB totally disappears at $\mathrm{Re}_r \ll \mathrm{Re}_d$ leaving a cone-shaped, near-axis flow—Fig. 3(d).

Sarpkaya[17] observed a similar transformation of VB into a conical wake-like pattern. The flow geometry and dynamics are very different in his and our cases: he studied a *turbulent* flow in a diverging vortex tube for a Reynolds number two orders of magnitude higher than that in our confined *laminar* flow. Despite this difference, the reason for VB disappearance might be common for both flows: the decrease in the swirl number SN, the ratio of swirl-to-meridional motion strengths.

There are different definitions of SN (depending on the flow), but in all cases, VB occurs as SN exceeds a threshold.[18] In the next section we provide some reasoning why the rod co-rotation decreases SN below the threshold and thus suppresses VB.

B. Discussion of the mechanism of VB suppression

1. The role of axial pressure gradient

First, we discuss the pressure distribution and start with the flow without the rod. For the flow without VB, Fig. 4 schematically (based on numerical simulations of Lopez[7]) shows (a) the distribution of velocity v_z along the axis; (b) a meridional streamline; (c) a curve of constant circulation (Γ); and (d) the distribution of pressure difference p_w-p_a at the same axial coordinate (indices *w* and *a* denote the sidewall and the axis).

Since v_z is zero at the ends (also $\partial v_z/\partial z=0$ by continuity and the no-slip condition), the fluid first accelerates and

Downloaded 14 Apr 2006 to 129.7.158.43. Redistribution subject to AIP license or copyright, see http://pof.aip.org/pof/copyright.jsp

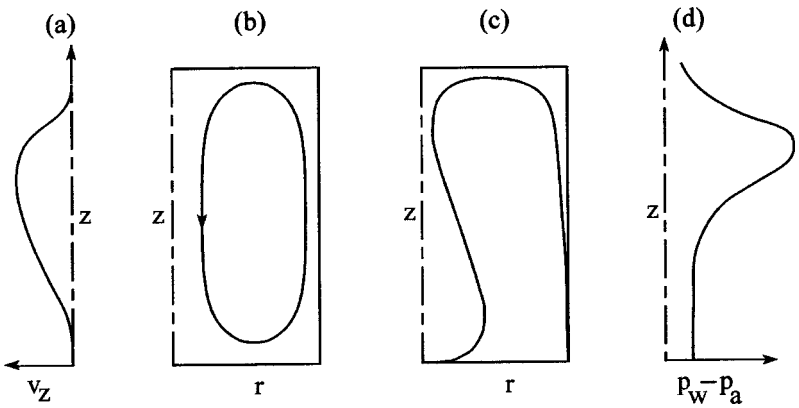

FIG. 4. Flow characteristics shown schematically when only the bottom disk rotates: (a) distribution of axial velocity v_z along the axis; (b) meridional streamline; (c) circulation contour in the meridional plane; and (d) distribution of pressure along the axis.

then decelerates as it flows along the axis. Hence pressure is minimum away from the ends discs—Fig. 4(d). We argue that such a pressure distribution is crucial for VB. According to the simulations of Lopez,[7] v_ϕ is higher (by about 10 times) than the radial and axial velocities. Due to this v_ϕ dominance, the radial pressure distribution is governed by the cyclostrophic balance, $\partial p/\partial r = \rho v_\phi^2/r$. To explain the pressure distribution in Fig. 4(d), let us first consider a z-independent swirling flow, e.g., the Rankine vortex.

2. Pressure distribution in the Rankine vortex

This one-dimensional swirling flow has the solid-body type rotation inside the vortex core and the potential-vortex rotation outside,

$$v_\phi = v_{\phi c} r/r_c \text{ for } 0 \leqslant r \leqslant r_c$$

and

$$v_\phi = v_{\phi c} r_c/r \text{ for } r \geqslant r_c, \tag{1}$$

where r_c is the core radius and $v_{\phi c}$ is the swirl velocity at $r = r_c$. Cyclostrophic balance yields that

$$p_a = p_w - \rho v_{\phi c}^2, \tag{2}$$

where p_w is the pressure at the sidewall (that is close to the pressure at infinity for $R_d \geqslant r_c$).

3. Pressure distribution in the container flow

In the closed-cylinder flow, the maximum swirl velocity in a normal-to-axis cross-section ($v_{\phi c}$) and p_a depend on z. In contrast, p_w is nearly z independent for the following reason. Consider the contour $\Gamma = r v_\phi = \text{const}$—Fig. 4(c)—that starts at the rim of the rotating disk and terminates on the same disk near the axis. This Γ-contour lies near but outside the boundary layer along the walls and the symmetry axis. Close to the sidewall, both streamlines and Γ-contours in the meridional plane are almost parallel to the sidewall. Then the Bernoulli integral (which can be applied outside the boundary layer) yields that pressure is nearly constant along the streamlines in the vicinity of the sidewall (recall that $v_\phi \geqslant v_r, r_z$). Thus, we can treat p_w as a constant in (2), and find p_a by exploring the dependence of $v_{\phi c}$ on z.

Where $\Gamma = r_c v_{\phi c}$ contour approaches the axis, p_a decreases according to (2) because $v_{\phi c}$ increases. Thus pressure attains its minimum near the top of the axis. As the Γ contour deviates from the axis [Fig. 4(c)], p_a increases because $v_{\phi c}$ decreases. This unfavorable axial pressure gradient, when sufficiently large, causes VB.

The flow again approaches the axis along the converging (i.e., downstream) part of bubble *i* in Fig. 2. This convergence results in acceleration of the swirl ("ice-dancer" effect) and in a new local minimum of pressure. Pressure recovery downstream of this minimum can cause the next VB. This explains three vortex rings observed in experiments (*i*–*iii* in Fig. 2). As we argue below, the rod co-rotation decreases the unfavorable pressure gradient along the axis and thus suppresses VB bubbles. To this end, consider first a flow induced by the rod rotation alone.

4. Features of control flow

To better understand how an additional flow affects the base flow, first examine features of the flow driven only by the rod. Both the meridional and swirl components of this flow provide control effects: the swirl induces centrifugal instability in the counter-rotation case (Sec. IV B) and the meridional motion suppresses VB in the co-rotation case (Sec. III B 5). The direct contribution of the additional co-rotation is small compared with that of the rod-generated meridional flow, whose two-cellular pattern is crucial for the control effect.

Figure 5 shows these two cells in a meridional plane at $\mathrm{Re}_r = 25$. The flow is symmetric with respect to the middle plane, $z = H/2$. Figure 6(a) shows the direction of the meridional flow visualized in Fig. 5. This direction is due to the "wall" effect, as explained below.

The centrifugal force and the radial pressure gradient are in balance outside the disk boundary layers. The centrifugal force vanishes at the top and bottom disks due to the no-slip condition, while the radial pressure gradient impressed on the disks drives the radial inflow (Ekman layer). This inflow turns near the disk center, producing a near-axis jet away from the disk. Two such jets collide in the mid-height region and yield a radial outflow. As this outflow meets the sidewall, it splits into two streams, upward and downward. Thus, the rod rotation induces a two-cell flow (more cells can appear due to the centrifugal instability for larger Re_r).

This rod-driven flow has a similar streamline pattern (but with the opposite direction) to the disk-driven flow studied by Lopez.[12] In that case, involving rotation of both disks, the

Downloaded 14 Apr 2006 to 129.7.158.43. Redistribution subject to AIP license or copyright, see http://pof.aip.org/pof/copyright.jsp

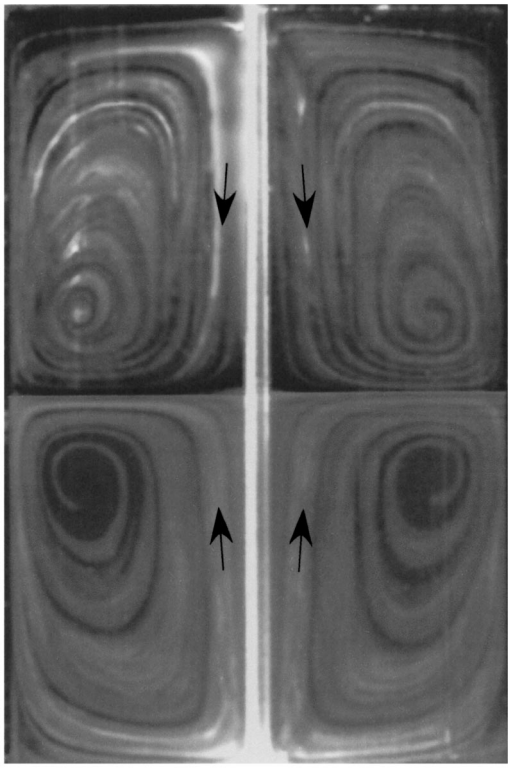

FIG. 5. Flow visualization when only the central rod rotates producing two large cells at $\mathrm{Re}_r=25$, $\mathrm{Re}_d=0$, and $H/R_d=3.25$. Arrows show the flow direction.

Karman ''pump'' induces the *diverging* flow near the disks. The opposite—*converging*—flow, induced near the disks by the rod rotation, is crucial for VB suppression, as we discuss below.

5. Co-rotation of the central rod and disk

Consider now the flow where both the rod and bottom disk rotate in the same direction. Although exact superposition of the motions is not expected (since Re is large and the nonlinear terms of the Navier–Stokes equations are involved), the flow patterns shown in Figs. 4(b) and 6(a) are approximately superimposed, yielding the pattern schematically shown in Fig. 6(b).

Since the flows in Figs. 4(b) and 6(a) have the same directions near the top disk, the velocity of the combined meridional flow is higher [emphasized by double arrow in Fig. 6(b)] than that shown in either Fig. 4(b) or 6(a). In contrast, the opposite directions of the flows in Figs. 4(b) and 6(a) decrease the velocity of the combined meridional flow near the bottom disk (the disk-induced motion dominates). Thus, the rod co-rotation decelerates the meridional flow near the bottom disk and accelerates near the top disk.

Consider now how the swirl distribution changes. The weakened meridional flow near the bottom decreases transport of angular momentum from the rotating disk, resulting in a slower swirl near the top. Figure 6(c) schematically shows contours $\Gamma=\mathrm{const}$ in the combined flow. Contour A ($\Gamma=\Gamma_r$, where Γ_r is the circulation value on the rod) starts at point E2 (the intersection point of the bottom disk and the sidewall) and ends at point E1 (the intersection point of the rod and the top disk). This contour separates the regions where $\Gamma<\Gamma_r$ (above A, e.g., contour B) and $\Gamma\geqslant\Gamma_r$ (below A, e.g., contours C and D). As Γ approaches its maximum value, contours similar to C and D collapse at E2.

According to the cyclostrophic balance, the weakened swirl decreases the maximum pressure drop [Fig. 6(d)] compared with that shown in Fig. 4(d). Furthermore, pressure along the axis tends to be more uniform due to the rod rotation that generates z-independent circulation. This pressure distribution, being more uniform along the lower part of the rod, first eliminates the vortex ring *iii* and then *ii* as Re_r increases (Fig. 3).

For bubble *i*, the swirl number SN plays a key role—VB occurs only if SN exceeds a threshold (Sec. III B 1). The rod rotation decreases SN by intensifying the meridional motion and by weakening swirl near the top disk. As Re_r increases, SN drops below its threshold, resulting in the disappearance of bubble *i*.

Thus, two factors—decrease in the axial pressure gradient and in SN—first suppress downstream vortex rings *iii* and *ii*, and then eventually suppress VB completely as the rod co-rotation increases. In contrast, the rod counter-rotation enhances VB as discussed below.

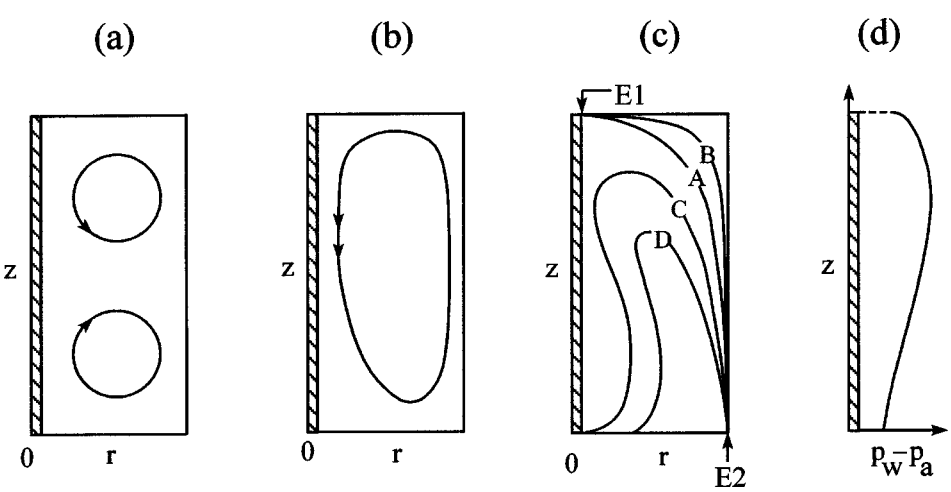

FIG. 6. Flow characteristics schematically showing: (a) meridional streamlines when only central rod rotates; (b) meridional streamlines for co-rotating disk and central rod; (c) circulation contours, $\Gamma=\mathrm{const}$, for (b); (d) distribution of pressure along the axis for (b).

Downloaded 14 Apr 2006 to 129.7.158.43. Redistribution subject to AIP license or copyright, see http://pof.aip.org/pof/copyright.jsp

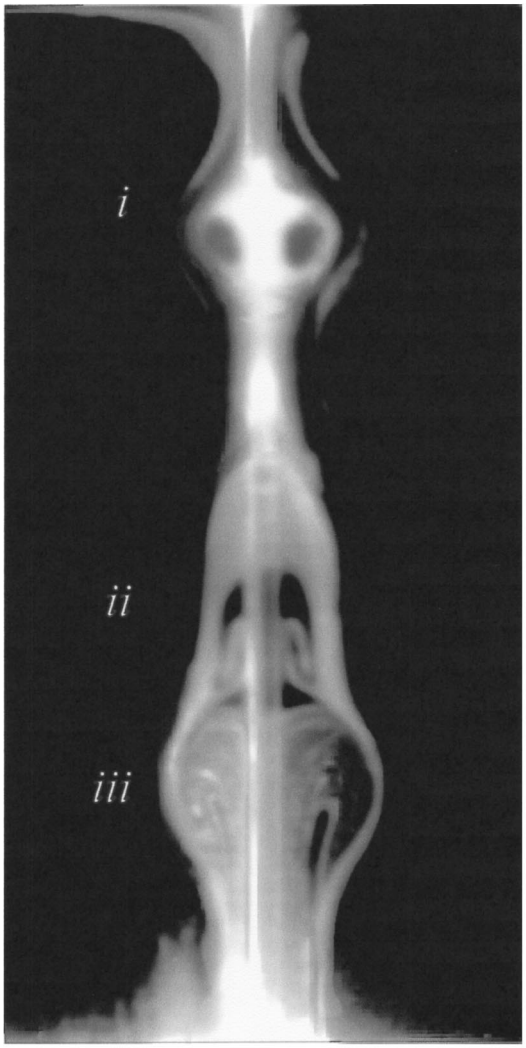

FIG. 7. Flow visualization for counter-rotating disk and central rod at $\mathrm{Re}_r=12$, $\mathrm{Re}_d=2720$, and $H/R_d=3.25$.

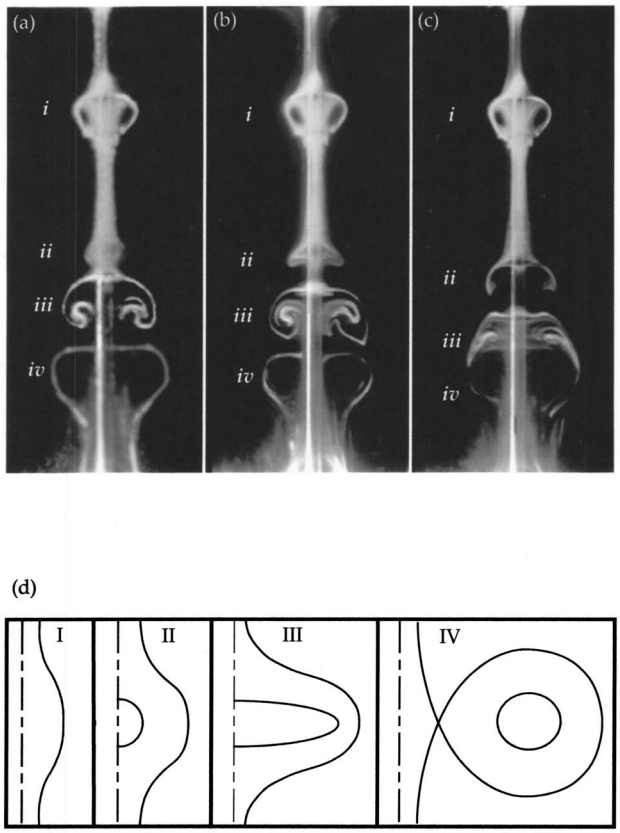

FIG. 8. Flow visualization, (a)–(c), showing time evolution of vortex breakdown bubbles for counter-rotating disk and central rod at $\mathrm{Re}_r=14.5$; (d) schematic of the development of the vortex ring *ii* via separation of streamlines from the axis (I–II) and streamline reconnection (III–IV).

IV. COUNTER-ROTATION

A. Experimental observations

With increasing Re_r of the rod counter-rotation, three distinct stages occur in the VB dynamics: (I) the vortex rings enlarge (this is a precursor of the centrifugal instability discussed in Sec. IV B), while the flow remains steady; (II) the top flow remains nearly steady, while the bottom flow exhibits a time-periodic oscillation with the repetitive disappearance and regeneration of vortex rings; (III) the entire flow becomes unsteady with a complex time evolution of all vortex rings. Figures 7–9 show stages I–III, respectively.

Figure 7 visualizes the change in the VB bubble geometry induced by the slow ($\mathrm{Re}_r=12$) rod counter-rotation (stage I). Comparison of Fig. 7 with Fig. 3(a1) (stationary rod) reveals that the counter-rotation significantly enlarges vortex ring *iii* and shifts it downstream.

Figure 8 illustrates stage II at $\mathrm{Re}_r=14.5$ by showing three characteristic phases (a)–(c) of the time-periodic dynamics of the downstream rings. Upstream vortex ring *i* remains nearly steady. In contrast, the downstream rings travel downstream, disappear as they meet the bottom disk (discussed below), and new vortices emerge near the height H/2. The new vortex appears as a blob of dye [as *ii* in Fig. 8(a)] that moves away from the axis [Fig. 8(b)] and rolls up [Fig. 8(c)]. Figure 8(d) schematically shows the new-vortex-ring development via streamline separation from the axis and reconnection. The expanding vortex (I–III) blocks the downflow which then penetrates along the axis (IV).

The previously formed vortex rings *iii* and *iv* [in Fig. 8(a)] move toward the bottom disk (the self-advection of the rings is opposite to the base flow, but the base flow dominates). As the meridional flow decelerates (until stagnation at the bottom disk), the rings approach each other [Fig. 8(b)], merge [Fig. 8(c)], and disappear via streamline reconnection [which is similar to that in Fig. 8(d), but in the opposite sequence—from IV to I], as the ring approaches the bottom disk. We can say that the ring and the boundary layer *merge* since their azimuthal vorticity is of the same sign. The ring disappearance in the boundary layer is a viscous effect in this low-Re flow.

Figure 9 shows the time evolution at stage III ($\mathrm{Re}_r=16.5$). Now the upstream vortex ring *i* also becomes strongly unsteady and the number of vortex rings increases. As the entire array of vortex rings (*i* through *iv*) moves downstream, the downstream vortex (*iv*) approaches the disk. Vortices *ii* and *iii* approach each other [Figs. 9(a)–9(c)] and merge [Figs. 9(d)–9(f)]. This ring dynamics in Fig. 9 is simi-

Downloaded 14 Apr 2006 to 129.7.158.43. Redistribution subject to AIP license or copyright, see http://pof.aip.org/pof/copyright.jsp

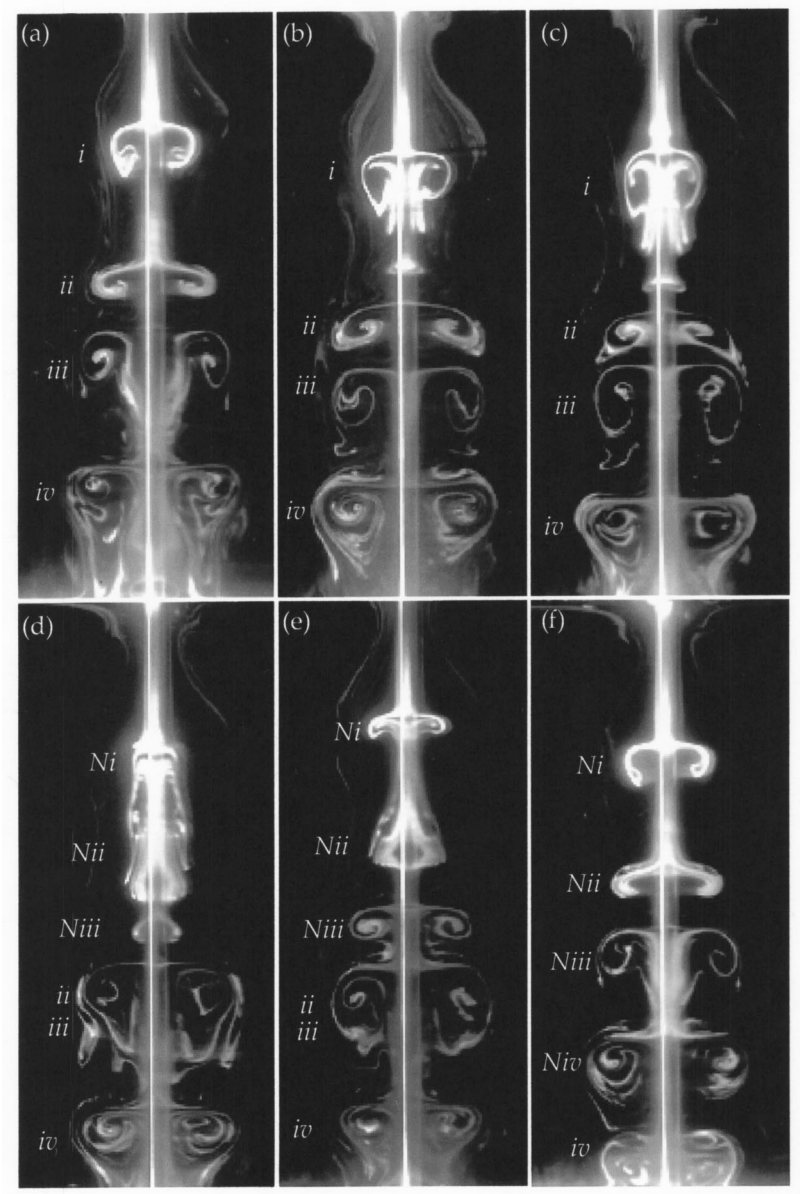

FIG. 9. Flow visualization of the time evolution of vortex breakdown bubbles for counter-rotating disk and central rod at $\mathrm{Re}_r=16.5$.

lar to that in Fig, 8. In contrast, the behavior of ring *i* is quite different. First, elongation of ring *i* [Figs. 9(a)–9(c)] occurs due to nonuniform axial velocities along the rod—the downstream part of the ring *i* moves faster than its upstream part (recall that the ring *i* does not move at all while the rings *ii* and *iii* move downstream in Fig. 8). After the elongation, ring *i* transforms into three (*Ni*–*Niii*; *N* denotes *new* rings) as Figs. 9(d)–9(f) show. First, ring *i* becomes a very elongated vortex pattern extending from *Ni* to *Niii* in Fig. 9(d). Then this pattern splits into three separated vortices—*Ni*, *Nii*, and *Niii* [Figs. 9(e) and 9(f)]. As rings *ii* and *iii* merge [Figs. 9(d) and 9(e)] into one, say ring *Niv* [Fig. 9(f)], and ring *iv* disappears in the boundary layer, the flow achieves a pattern close to that in Fig. 9(a) [with the rings *Ni*–*Niv* replacing *i*–*iv*], and the process reiterates.

It is striking that even a weak ($\mathrm{Re}_r \ll \mathrm{Re}_d$) near-axis counter-rotation can cause dramatic changes in the topology and in the time dependence of a much stronger outer swirling flow. Compare the effects of co-rotation, which completely suppresses VB at $\mathrm{Re}_r=29$, with the effects of counter-rotation, which induces strong unsteadiness in the flow at $\mathrm{Re}_r=16.5$. The formation of multiple traveling vortex rings essentially diffuses the species concentration away from the axis much more rapidly than the original swirling flow [compare Figs. 3(a1) and 9]. Such a feature is favorable for combustion applications and for destroying wing-tip vortices of aircraft.

Now we discuss how the counter-rotation induces the flow instability.

B. Discussion of the counter-rotation effect

Here we attempt to explain why the rod counter-rotation produces the unsteady flow in contrast to the steady flow for rod co-rotation at the same values of Re_d and Re_r (as well as without the rod or with the stationary rod). The reason lies in the different stability features of the co- and counter-rotating flows as explained below.

Downloaded 14 Apr 2006 to 129.7.158.43. Redistribution subject to AIP license or copyright, see http://pof.aip.org/pof/copyright.jsp

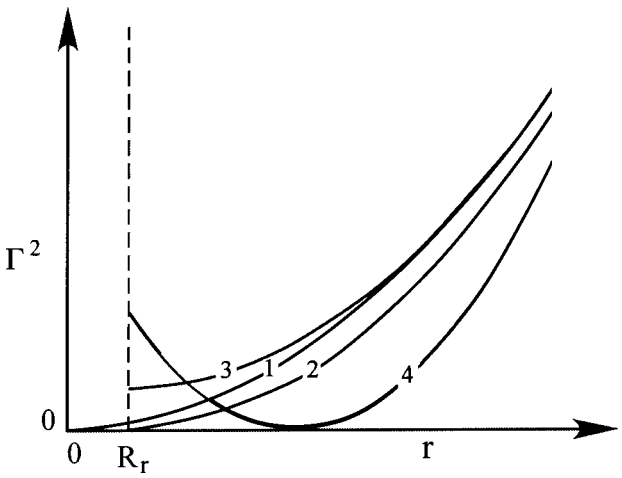

FIG. 10. Schematic of the squared circulation (Γ^2) dependence on the distance from the axis r for a flow without the rod (1) and with the stationary (2), co-rotating (3), and counter-rotating (4) rod.

The appearance of VB bubbles is a manifestation of internal flow separation—separation of streamlines from the axis causing the reversal of the axial velocity—which can occur without instability. In the case when there is no rod and only an end disk rotates, numerical simulations of the base flow and studies of its stability[19] clearly show this. The instability, in general, occurs at a different Reynolds number than that for the appearance of VB and leads to a time-oscillating flow not necessarily involving VB. These theoretical predictions[19] as well as the following studies of three-dimensional instabilities,[20–22] flow topology,[23] and bifurcations[24] agree with experimental observations. Ranges of Re_d for which VB and the instability occur may overlap or separate depending on H/R_d.

We reiterate that the change in flow topology related to the appearance or disappearance of (axisymmetric and steady) VB bubbles can occur without any instability and bifurcation. In contrast, the transition from steady to time-oscillating flows always develops via instability and (Hopf) bifurcation. Also, the merger of vortex rings (e.g., *ii* and *iii* in Fig. 9) may involve the secondary (subharmonic) instability. Both of these features—oscillations and merger—appear due to the rod counter-rotation that, therefore, stimulates instability.

In our experiment, where H/R_d and Re_d are fixed, the critical Reynolds number for the instability depends only on the rod rotation. We view that the instability mechanism of counter-rotation is centrifugal. According to the Rayleigh criterion, Γ^2 must increase with the distance from the axis (r) for the centrifugal stability of a swirling flow. The near-axis flows without the rod, with the stationary rod, and with the co-rotating rod satisfy the Rayleigh condition while the flow with the counter-rotating rod *does not* satisfy, as Fig. 10 illustrates. It is important that Γ changes its sign in the counter-rotation case, and, therefore, Γ^2 first decreases to zero and then increases as r increases (curve 4 in Fig. 10). As Re_r increases, the decrease in $\Gamma^2(r)$ near the rod becomes stronger resulting in the centrifugal instability. This instability indeed occurs near the rod, as Fig. 8 shows where ring *ii* appears on the rod and then expands as time increases.

The counter-rotational flow studied by us and the Taylor–Couette flow have common features typical of the centrifugal instability: (a) radial profile of swirl is favorable for instability and (b) vortex rings develop. The difference is that (I) adjacent Taylor vortices have meridional circulation of opposite signs, whereas here the vortex rings have circulation of the same sign (which is opposite to that of the base flow) and (II) the Taylor vortices are steady when they first appear, whereas here the vortex rings travel. Both the differences are due to the presence of base meridional flow in our case.

The azimuthal vorticity produced near the rod due to no-slip is opposite to that away from the rod. This disallows near-axis vortex rings having the same direction of meridional circulation as produced by the rotating disk, but stimulates rings of the opposite-to-the-base-flow circulation. This explains the feature (I).

Near the axis, the flow direction is opposite to that of the ring's self-advection (this makes possible steady rings in a stable flow). The maximum velocity of upward flow near the sidewall, by continuity, is smaller than that of downward flow near the axis. The higher velocity of the downward flow and the centrifugal instability induce wave disturbances traveling and transporting the vortex rings toward the bottom disk. This explains the feature (II).

V. DISCUSSION

Here we compare our results with those obtained by Mullin *et al.*[16] and address remarks concerning precedence and contradictory conclusions. Our concept to use a thin rotating rod for VB control[25] and some preliminary results[26] precede Ref. 16 as our work was completed much earlier. Also, the main thrusts are different: we focus on VB control while Mullin *et al.* address the similarity in the appearance of stagnation points on the free core and near straight and sloped walls.

Mullin *et al.*[16] found that "the addition of a small straight cylinder along the centerline of a cylindrical container of fluid with one rotating wall has no qualitative effect on the appearance of stagnation points on the core of induced vortex. This is true regardless of whether the central cylinder is rotating or stationary."

Our results contradict this statement because the angular velocities of the rod rotation required for VB control are significantly higher than those used by Mullin *et al.*[16] We have found that the total VB suppression by co-rotation occurs at the rod-to-disk angular velocity ratio $\Omega_r/\Omega_d \approx 6$ while $\Omega_r/\Omega_d \leqslant 1$ in Ref. 16. The flow becomes unsteady at $|\Omega_r/\Omega_d| > 3$ in our counter- rotation case while Mullin *et al.* address no counter-rotation effect.

To achieve VB control in the Mullin *et al.* case, $|\Omega_r/\Omega_d|$ should be higher than 6 for co-rotation and greater than 3 for counter-rotation. The reason is the different parameter values: the smaller aspect ratio (1.6 in Ref. 16 vs 3.25 in our case), Reynolds number Re_d (2000 vs 2720), and the outer-to-inner cylinder-radius ratio (10 vs 24). These differences make the flow less sensitive to a control action (due to stron-

Downloaded 14 Apr 2006 to 129.7.158.43. Redistribution subject to AIP license or copyright, see http://pof.aip.org/pof/copyright.jsp

ger viscous diffusion and dissipation) in the Mullin *et al.* case. For instance, they did not observe any qualitative difference between the flows without and with the rod at $\mathrm{Re}_r=22$ (that corresponds to $R=200$ in Ref. 16) while we observe significant VB suppression even at $\mathrm{Re}_r=21$ [compare Fig. 3(c1) with Figs. 2 and 3(a1)].

Our motivation for the parameter choice was to be as close as possible to practical flows (where both Re and aspect ratio are large) with minimal intrusion (small rod-to-disk radius ratio). For this reason, we used Re_d and the aspect ratio as high as we could reach with steady VB in our facility. Also we chose the rod radius to be close to that of the vortex core. Because of such small radius, the angular velocity is higher in our case compared with Ref. 16 at the same value of Re_r. This explains why VB control requires larger angular velocities than that used by Mullin *et al.*[16]

VI. CONCLUSIONS

We have shown that an addition of swirl near the axis of a swirling flow is an effective means to either suppress or enhance VB. Here we apply such a control strategy to a flow in a closed cylinder driven by its rotating disk. A thin central rotating rod provides the additional (control) swirl. The flow appears very sensitive to the direction of rod rotation. Co-rotation retains a steady flow, suppresses VB bubbles, and induces a conically diverging near-axis pattern devoid of any flow reversal near the axis. Counter-rotation makes the flow unsteady and stimulates the appearance and merger of traveling vortex rings. Simple analytical arguments explain the effect of the co-rotation in terms of decreased unfavorable pressure gradient and the swirl number. We argue that counter-rotation induces the centrifugal instability resulting in the VB enhancement.

Thus, our study has revealed features which can be exploited for VB control in practical flows. For example, an additional co- or counter-rotational swirl applied in the vortex core can help to avoid VB over delta wings or to diffuse the long-range trailing vortices of aircraft. In vortex burners, an additional counter-rotating flow induced near the axis can enhance mixing, improve combustion, and reduce harmful emissions. It is clear that in practical systems, rod rotation may not be feasible. In that case, an additional near-axis swirling jet could replace the rod to achieve similar effects — suppression or stimulation of vortex breakdown.

ACKNOWLEDGMENT

This research was partially supported by NSF Grant No. CTS 9904328.

[1] P. G. Saffman, *Vortex Dynamics* (Cambridge University Press, Cambridge, 1992).
[2] M. P. Escudier, ''Vortex breakdown: observations and explanations,'' Prog. Aerosp. Sci. **25**, 189 (1988).
[3] A. K. Gupta, D. G Lilley, and N. Syred, *Swirl Flows* (Abacus, New York, 1984).
[4] V. Shtern and F. Hussain, ''Hysteresis in swirling jets,'' J. Fluid Mech. **309**, 1 (1996).
[5] A. Schmucker and K. Gersten, ''Vortex breakdown and its control on delta wings,'' Fluid Dyn. Res. **3**, 268 (1988).
[6] M. P. Escudier, ''Observation of the flow produced in a cylindrical container by a rotating endwall,'' Exp. Fluids **2**, 189 (1984).
[7] J. M. Lopez, ''Axisymmetric vortex breakdown. Part 1. Confined swirling flows,'' J. Fluid Mech. **221**, 533 (1990).
[8] A. Spohn, N. Mory, and E. J. Hopfinger, ''Observations of vortex breakdown in an open cylindrical container with a rotating bottom,'' Exp. Fluids **14**, 70 (1993).
[9] D. L. Young, H. J. Sheen, and T. Y. Hwu, ''Period-doubling route to chaos for a swirling flow in an open cylindrical container with a rotating disk,'' Exp. Fluids **18**, 389 (1995).
[10] K. G. Roesner, ''Recirculation zones in a cylinder with rotating lid,'' in *Topological Fluid Mechanics*, edited by H. K. Moffatt and A. Tsinober (University of Cambridge, Cambridge, 1990), p. 699.
[11] D. T. Valentine and C. C. Jahnke, ''Flow induced in a cylinder with both endwalls rotating,'' Phys. Fluids **6**, 2702 (1994).
[12] J. M. Lopez, ''Unsteady swirling flow in an enclosed cylinder with reflectional symmetry,'' Phys. Fluids **7**, 2700 (1995).
[13] M. Goldshtik, H. S. Husain, and F. Hussain, ''Loss of homogeneity in a suspension by kinematic action,'' Nature (London) **357**, 141 (1992).
[14] R. Bradlaw, ''A flow visualization study of some flow patterns found in the vortex breakdown produced in a closed cylindrical container,'' BSME Honors thesis, University of Houston, Houston, 1993.
[15] J. C. F. Pereira and J. M. M. Sousa, ''Confined vortex breakdown generated by a rotating cone,'' J. Fluid Mech. **385**, 287 (1999).
[16] T. Mullin, J. J. Kobine, S. J. Tavener, and K. A. Cliffe, ''On the creation of stagnation points near straight and sloped walls,'' Phys. Fluids **12**, 425 (2000).
[17] T. Sarpkaya, ''Turbulent vortex breakdown,'' Phys. Fluids **7**, 2301 (1995).
[18] V. Shtern and F. Hussain, ''New features of swirling jets,'' Phys. Fluids **12**, 2868 (2000).
[19] A. Yu. Gelfgat, P. Z. Bar-Yoseph, and A. Solan, ''Stability of confined swirling flow with and without vortex breakdown,'' J. Fluid Mech. **311**, 1 (1996).
[20] A. Yu. Gelfgat, P. Z. Bar-Yoseph, and A. Solan, ''Three-dimensional instabilities of axisymmetric flow in a rotating lid-cylinder enclosure,'' J. Fluid Mech. **438**, 363 (2001).
[21] E. Serre and P. Bontoux, ''Vortex breakdown in a three-dimensional swirling flow,'' J. Fluid Mech. **459**, 347 (2002).
[22] F. Sotiropulos and Y. Venticos, ''The three-dimensional structure of confined swirling flows with vortex breakdown,'' J. Fluid Mech. **426**, 155 (2001).
[23] M. Brons, L. K. Voigt, and J. N. Sorensen, ''Streamline topology of steady axisymmetric vortex vreakdown in a cylinder with co- and counter-rotating end-covers,'' J. Fluid Mech. **401**, 275 (1999).
[24] M. Brons, L. K. Voigt, and J. N. Sorensen, ''Topology of vortex breakdown bubbles in a cylinder with rotating bottom and free surface,'' J. Fluid Mech. **428**, 133 (2001).
[25] H. Husain, V. Shtern, and F. Hussain, ''Control of vortex breakdown,'' Bull. Am. Phys. Soc. **41**, 1764, FB 1 (1996).
[26] H. Husain, V. Shtern, and F. Hussain, ''Control of vortex breakdown using vortex generators,'' AIAA Pap. 97-1879 (1997).

Downloaded 14 Apr 2006 to 129.7.158.43. Redistribution subject to AIP license or copyright, see http://pof.aip.org/pof/copyright.jsp